NeuroImage 184 (2019) 56–67

Contents lists available at ScienceDirect

NeuroImage

journal homepage: www.elsevier.com/locate/neuroimage

A realistic, accurate and fast source modeling approach for the EEG forward problem

Tuuli Miinalainen [a,c,d,e], Atena Rezaei [a,*], Defne Us [a,b], Andreas Nüßing [c,d], Christian Engwer [d], Carsten H. Wolters [c], Sampsa Pursiainen [a]

[a] Laboratory of Mathematics, Tampere University of Technology, P.O. Box 692, 33101, Tampere, Finland
[b] Laboratory of Signal Processing, Tampere University of Technology, Tampere, Finland, P.O. Box 553, 33101, Tampere, Finland
[c] Institute for Biomagnetism and Biosignalanalysis, University of Münster, Germany, Malmedyweg 15, D-48149, Münster, Germany
[d] Institute for Computational and Applied Mathematics, University of Münster, Germany, Einsteinstrasse 62, D-48149, Münster, Germany
[e] Department of Applied Physics, University of Eastern Finland, P.O.Box 1627, FI-70211 Kuopio, Finland

ARTICLE INFO

Keywords:
Electroencephalography (EEG)
Finite element method (FEM)
Divergence conforming vector fields
Focal sources
DUNE toolbox

ABSTRACT

The aim of this paper is to advance electroencephalography (EEG) source analysis using finite element method (FEM) head volume conductor models that go beyond the standard three compartment (skin, skull, brain) approach and take brain tissue inhomogeneity (gray and white matter and cerebrospinal fluid) into account. The new approach should enable accurate EEG forward modeling in the thin human cortical structures and, more specifically, in the especially thin cortices in children brain research or in pathological applications. The source model should thus be focal enough to be usable in the thin cortices, but should on the other side be more realistic than the current standard mathematical point dipole. Furthermore, it should be numerically accurate and computationally fast. We propose to achieve the best balance between these demands with a current preserving (divergence conforming) dipolar source model. We develop and investigate a varying number of current preserving source basis elements n ($n = 1,\ldots,n = 5$). For validation, we conducted numerical experiments within a multi-layered spherical domain, where an analytical solution exists. We show that the accuracy increases along with the number of basis elements, while focality decreases. The results suggest that the best balance between accuracy and focality in thin cortices is achieved with $n = 4$ (or in extreme cases even $n = 3$) basis functions, while in thicker cortices $n = 5$ is recommended to obtain the highest accuracy. We also compare the current preserving approach to two further FEM source modeling techniques, namely partial integration and St. Venant, and show that the best current preserving source model outperforms the competing methods with regard to overall balance. For all tested approaches, FEM transfer matrices enable high computational speed. We implemented the new EEG forward modeling approaches into the open source *duneuro* library for forward modeling in bioelectromagnetism to enable its broader use by the brain research community. This library is build upon the *DUNE* framework for parallel finite elements simulations and integrates with high-level toolboxes like *FieldTrip*. Additionally, an inversion test has been implemented using the realistic head model to demonstrate and compare the differences between the aforementioned source models.

1. Introduction

In electroencephalography (EEG) source analysis, brain activity is to be detected via voltage measurements on the scalp surface which leads to the so-called *EEG inverse problem* (Brette and Destexhe, 2012). The major advantages of the EEG include, for example, its high temporal resolution and noninvasive nature. That is, the measurements can be carried out fully outside of the head without a need to touch the brain itself or to apply high-intensity external electromagnetic fields present, for example, in functional magnetic resonance imaging (fMRI) (Brette and Destexhe, 2012). Because of these reasons, EEG source analysis is now one of the standard methods also in children, infant and even neonate brain research (see, e.g. (Hämäläinen et al., 2015; Roche-Labarbe et al., 2008)).

The EEG inverse problem is ill-posed, i.e., its solution is non-unique and sensitive to noise and modeling errors. Consequently, the reconstruction process necessitates clinical, physical and neurophysiological *a*

* Corresponding author.
E-mail address: atena.rezaei@tut.fi (A. Rezaei).

https://doi.org/10.1016/j.neuroimage.2018.08.054
Received 20 February 2018; Received in revised form 9 August 2018; Accepted 22 August 2018
Available online 28 August 2018

priori knowledge (Brette and Destexhe, 2012). It is also strongly relying on the accuracy of the solution to the *EEG forward problem*, where the electric potentials, generated by the impressed primary current sources in the brain, have to be simulated using a realistic head volume conductor model (Brette and Destexhe, 2012).

This paper aims at developing, implementing and validating a more accurate and realistic EEG forward approach. We want to strive for head volume conductor models that go beyond the standard three compartment (skin, skull, brain) approach and take brain tissue inhomogeneity, e.g., gray and white matter and cerebrospinal fluid (CSF), into account.

In order to solve the EEG forward problem in such realistic geometries, numerical approaches are needed and to guarantee the accuracy of modeling the neural currents, the source needs to be placed into the thin cortical layer which is on average only slightly more than 2 mm thick (Griffis et al., 2016; Fischl and Dale, 2000; McGinnis et al., 2011). That is, the focality of the source model is essential (Brette and Destexhe, 2012; Pursiainen et al., 2016). The boundary element method (BEM), which is currently the most extensively used numerical EEG forward modeling technique, hardly allows modeling of such tissue conductivity inhomogeneity. Although it is possible to include the distinction of tissue structures with BEM, this would lead to heavy computational complexity and significantly high memory demand (Brette and Destexhe, 2012; Vorwerk et al., 2012). A broader overview of EEG forward modeling techniques can be found, for example, in (Brette and Destexhe, 2012).

In this article, the forward problem is approached via the finite element method (FEM) (Braess, 2001). The FEM is known to provide an accurate modeling framework with advanced computational features for several applied fields of science and engineering. The FEM has also been proven to be a feasible method for the EEG forward problem (Marin et al., 1998; Haueisen et al., 2002; Ramon et al., 2006), where the finite element (FE) mesh can be generated based on a precise MRI based head geometry including its internal surfaces and complex 3D conductivity structures (Papageorgakis, 2017; Pursiainen et al., 2016). It has been shown that very fine 3D structures need to be modeled, e.g., the CSF and compact and spongious bone (Papageorgakis, 2017; Montes-Restrepo et al., 2014). The FEM allows modeling of such complex geometries and, consequently, it has a great potential regarding future EEG applications.

As the reference model for validation, we use a multi-layer sphere model and a classical mathematical point dipole determined by its location, orientation and magnitude, since analytical solutions have been derived for it (de Munck and Peters, 1993). However, it was also already shown that the point dipole source results in small, but systematic depth localization errors due to its over-focal nature when compared to a more realistic and slightly more extended source model (de Munck et al., 1988). The point dipole can also be modeled with its full focality in a FEM framework using the so-called *subtraction approach*, but it is known that this approach is computationally expensive and that numerical errors might get significant on the boundaries in thin cortices, where sources are very close to the next conductivity discontinuity (Bertrand et al., 1991; Awada et al., 1997; Marin et al., 1998; Schimpf et al., 2002; Drechsler et al., 2009). The computational costs of all direct approaches presented in this paper including the H(div) technique are very low compared to the computationally expensive full subtraction approach (Drechsler et al., 2009) and somewhat similar to each other, since it is considerably lower than what is needed for generating the transfer matrix.

In this paper, we will study current preserving H(div) source models, which are slightly less focal than the standard mathematical point dipole, but, as will be shown, well-localized enough to be embedded in the thin cortical structures (Griffis et al., 2016; Fischl and Dale, 2000; McGinnis et al., 2011) and the even thinner cortices as needed especially in children brain research (Li et al., 2014) and/or pathological situations (Seitz et al., 2014). The issues and sensitivity of the classical St. Venant (Buchner et al., 1997; Toupin, 1965) and partial integration (Yan et al., 1991; Weinstein et al., 2000) source models regarding these situations has recently been observed and studied in (Nüßing, 2018; Medani, 2016; Medani et al., 2015). The simplest case of the current preserving H(div) approach is the Whitney (Raviart-Thomas) source model (Bauer et al., 2015; Pursiainen, 2012) in which the linear Whitney functions constitute the sources. Recent studies (Pursiainen et al., 2016; Vorwerk et al., 2017; Tanzer et al., 2005) have shown that the generalized H(div) model results in a focal and highly exact solution for the EEG forward problem. It is also a fast technique compared to the full subtraction approach (Drechsler et al., 2009) as the source modeling process requires effectively the same computational cost as in the simple classical methods (Bauer et al., 2015). That is, the source field can be obtained in a fraction of the time which is required to evaluate the transfer matrix.

In this study, we implemented and validated an adaptable solver into *duneuro*[1] (Nüßing, 2018; Nüßing et al., 2016; Engwer et al., 2017; Vorwerk et al., 2017), an open source C++ library for solving forward problems in bioelectromagnetism applications belonging to the open source toolbox *DUNE*[2] (Blatt and Bastian, 2007; Blatt et al., 2016; Bastian et al., 2008a; b). *DUNE* is currently being developed for various different applications of partial differential equations. For its modular programming interface, it provides a suitable platform for EEG/MEG computations where the geometrical complexity of the biological tissue structures has to be taken into account in the modeling process. As a novel design, we explore how the number of the elements in the source configuration affects the modeling accuracy. Our interest is, in particular, in the areas close to the outer gray matter boundary, where the discontinuity in the electrical conductivity distribution easily causes forward errors. In order to prevent those, the element patch of the source configuration needs to be restricted to avoid an overlap with the cerebrospinal fluid (CSF) compartment.

In the numerical experiments, we find out how the H(div) model performs with respect to a varying number of current preserving source basis elements n ($n = 1, \ldots, n = 5$) in comparison to the St. Venant and partial integration method. We also give a computed example on how the adaptivity with respect to n potentially affects source localization inverse estimates in a realistic multi-compartment head model. The results suggest that the best H(div) source model outperforms the competing methods with regard to overall balance and that it is especially well-suited for situations in which the focality of the source model is essential such as on the boundaries. The best balance between accuracy and focality in thin cortices is achieved by *adaptive H(div)* $n = 4$ (or in extreme cases even $n = 3$) basis functions, while in thicker cortices $n = 5$ is recommended to obtain the highest accuracy by *non-adaptive H(div)*.

This paper is structured as follows: The materials and methods are described in Section 2 including the H(div) source model, its implementation into *duneuro*, and numerical evaluation process. After that, the results of the numerical experiments are presented in Section 3 and discussed in Section 4. Finally, the conclusions are summed up in Section 5.

2. Materials and methods

2.1. Forward model

The EEG forward problem is to solve the electric potential field u on the surface $\partial\Omega$ of the head model (domain) Ω with a given source current density $\vec{J}^P$ and a conductivity tensor distribution σ that is known to be point-wise symmetric and positive definite (Brette and Destexhe, 2012). Applying the quasi-static approximation.

The electric potential u can be modeled using the following Poisson type equation equipped with the zero Neumann boundary condition. That is, the normal current density on the surface equals zero, as the head is electrically isolated (Hallez et al., 2007; Brette and Destexhe, 2012):

[1] *duneuro*: http://www.duneuro.org.
[2] *DUNE*: https://www.dune-project.org.

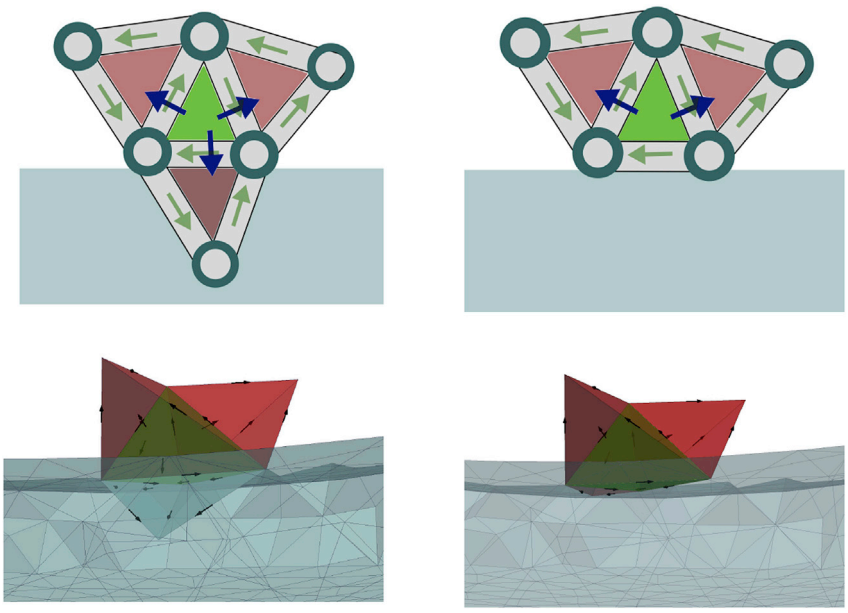

Fig. 1. The five-element source configuration near the gray matter boundary. The top row includes a two-dimensional schematic illustration of the dipolar FI (dark blue) and EW (light green) sources. The images on the left side present the scenario where the sources are not limited in the gray matter area. The restricted version is presented in the images on the right side, where elements not belonging to the gray matter are excluded to prevent the forward errors.

$$\nabla \cdot (\sigma \nabla u) = \nabla \cdot \vec{J}^{P} \quad \text{in} \quad \Omega \quad \text{with} \quad (\sigma \nabla u) \cdot \vec{n} = 0 \quad \text{on} \quad \partial\Omega \tag{1}$$

Multiplying both sides with a test function v, and taking the partial integral over Ω results in the weak form (Pursiainen et al., 2016)

$$\int_{\Omega} \nabla v \cdot (\sigma \nabla u) dV = -\int_{\Omega} v\left(\nabla \cdot \vec{J}^{P}\right) dV \quad \text{for all} \quad v \in H^1(\Omega) \tag{2}$$

which consists of two parts: the operator part on the left side and source part on the right side. Here, $H^1(\Omega)$ denotes the Sobolev space containing the functions that have square integrable first-order partial derivatives, i.e., that are in $L_2(\Omega)$. If the divergence of the primary current density is square integrable, i.e., if $\vec{J}^{P} \in H(\mathrm{div}) = \{\vec{w} | \nabla \cdot \vec{w} \in L^2(\Omega)\}$, the electric potential u determined by the weak form is unique up to choosing the ground level (Drechsler et al., 2009). Namely, $L^2(\Omega)$ means the primary current field is a finite energy.

The domain Ω is subdivided into a set of tetrahedral finite elements (FEs) (Braess, 2001). It is assumed that the potential u belongs to a subspace $S \in H^1(\Omega)$ that is spanned by the FE basis functions. The potential distribution is approximated as the finite sum $u_h = \sum_{i=1}^{N} z_i \psi_i$ in which $\psi_1, \psi_2, \ldots, \psi_N \in H^1(\Omega)$ are piecewise linear nodal basis functions. Similarly, the primary current distribution is modeled with the H(div) approach via $\vec{J}_h^{P} = \sum_{j=1}^{K} x_j \vec{w}_j$ where $\vec{w}_1, \vec{w}_2, \ldots, \vec{w}_K \in H(\mathrm{div})$ are the divergence conforming basis functions (Pursiainen et al., 2016). Associating u_h and $\vec{J}_h^{P}$ with coordinate vectors $\mathbf{z} = (z_1, z_2, \ldots, z_N)$ and $\mathbf{x} = (x_1, x_2, \ldots, x_K)$, the weak form turns to a solvable linear system $\mathbf{Az} = \mathbf{Gx}$ where $\mathbf{A} \in \mathbb{R}^{(N \times N)}$ and $\mathbf{G} \in \mathbb{R}^{(N \times K)}$ with

$$A_{i,j} = \int_{\Omega} \nabla \psi_j \cdot (\sigma \nabla \psi_i) dV \quad \text{and} \quad G_{i,j} = \int_{\Omega} \psi_i \left(\nabla \cdot \vec{w}_j\right) dV. \tag{3}$$

The measurement vector $\mathbf{y}$ for the electrode voltages can be formed as $\mathbf{y} = \mathbf{RA}^{-1}\mathbf{Gx} = \mathbf{Tf}$, in which $\mathbf{f} = \mathbf{Gx}$ is a load vector which represents the activity in the brain and $\mathbf{T} = \mathbf{RA}^{-1}$ is a so-called transfer matrix (Gencer and Acar, 2004; Drechsler et al., 2009). In addition, the matrix $\mathbf{R}$ is a restriction operator for picking the skin potentials at the electrode positions (Pursiainen et al., 2016). The matrix $\mathbf{R}$ denotes the zero potential level, here the mean of the measurements $\mathbf{y}$. The elements of matrix $\mathbf{R}$ are defined as follows: If the ℓ-th electrode on the boundary $\partial\Omega$ is positioned at the i_ℓ-th node, $R_{\ell, i_\ell} = 1 - 1/L$. Also, if $\ell \neq j$, $R_{\ell, i_j} = -1/L$. Finally, $R_{\ell, j} = 0$, if the j-th node is not associated with any electrode(Pursiainen et al., 2016).

2.2. Dipolar sources

In this study, the primary source currents are constructed using synthetic dipolar sources for the linear and quadratic basis functions of $H(\mathrm{div})$ (Ainsworth and Coyle, 2003). The dipolar moment $\vec{q}_{\vec{w}}$ of the basis function $\vec{w}$ is defined as $\vec{q}_{\vec{w}} = \int_{\Omega} \vec{w}\, dV$. In a tetrahedral FE mesh, the moment and position of a synthetic dipole can be expressed as follows:

$$\vec{q}_{\vec{w}} = \frac{\vec{r}_{P_j} - \vec{r}_{P_i}}{\left\| \vec{r}_{P_j} - \vec{r}_{P_i} \right\|} \quad \text{and} \quad \vec{r}_{\vec{w}} = \frac{1}{2}\left(\vec{r}_{P_i} + \vec{r}_{P_j}\right) \tag{4}$$

in which $\vec{r}_{P_i}$ and $\vec{r}_{P_j}$ are the position vectors of mesh nodes P_i and P_j (Pursiainen et al., 2016). The right-hand side matrix $\mathbf{G}$ can be formed as

$$G_{\psi, \vec{w}} = \int_{\Omega} \psi (\nabla \cdot \vec{w}) dV = \frac{s_{\{\psi, P_j\}} - s_{\{\psi, P_i\}}}{\left\| \vec{r}_{P_j} - \vec{r}_{P_i} \right\|} \tag{5}$$

for a given pair ψ, $\vec{w}$ of the basis functions with $s_{\{\psi, P\}} = 1$, if ψ corresponds to node P and $s_{\{\psi, P\}} = 0$, otherwise. For more detailed formulation, see e.g., (Pursiainen et al., 2016; Bauer et al., 2015).

For the linear $H(\mathrm{div})$ basis functions, the resulting source dipole is defined by nodes P_i and P_j that are located on the opposing sides of a shared face in an adjacent tetrahedron pair. This is referred to as the face intersecting (FI) orientation. For the quadratic basis, P_i and P_j are attached by an edge, leading to an edgewise (EW) orientation. As shown later on, various source configurations can be formed by taking different combinations of these dipoles.

For constructing the load vector $\mathbf{f} = \mathbf{Gx}$ for an arbitrary dipole position $\vec{r}$ and a moment $\vec{p}$, an interpolation technique needs to be applied. That is, to find coefficients $\mathbf{c} = (c_1, c_2, \ldots, c_M)$ such that

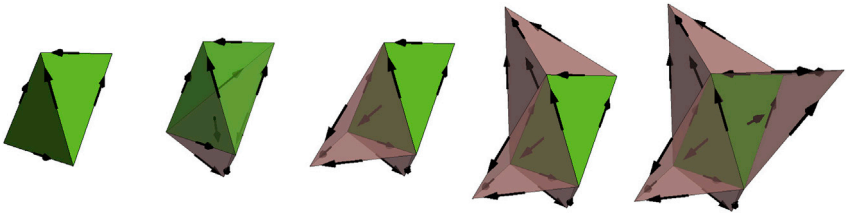

Fig. 2. From left to right, respectively: The element patch of the source configurations for $n = 1, 2, \ldots, 5$ elements with FI and EW dipoles. In each configuration, the center element is marked with green.

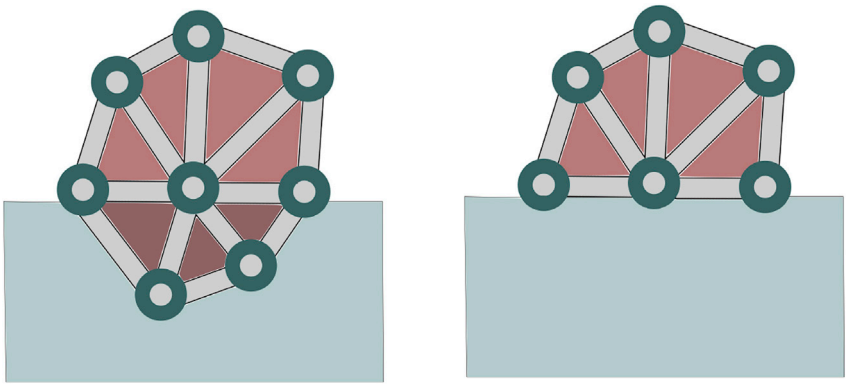

Fig. 3. A schematic illustration of the ball-like St. Venant source element patch. On the boundary of the gray matter approximately one half of the elements (darker red color in the image on the left side) are taken out of the final configuration (right) in its adapted version.

$$\vec{p} \approx \sum_{\ell=1}^{M} c_\ell \vec{q}_{\vec{w}_\ell} \quad \text{and} \quad \vec{r} \approx \sum_{\ell=1}^{M} c_\ell \vec{r}_{\vec{w}_\ell}. \tag{6}$$

In this study, we use the position based optimization (PBO) technique (Bauer et al., 2015) in which the preference is on $\vec{p}$ over $\vec{r}$. With PBO, the coefficients c_ℓ are found by solving the linear system $\min_{\mathbf{c}} \sum_{\ell=1}^{M} c_\ell^2 \omega_\ell^2$ subject to $\mathbf{Qc} = \mathbf{p}$. Here ω_ℓ is a weighting coefficient, defined as $\omega_\ell = \left\| \vec{r}_{\vec{\omega}_\ell} - \vec{r} \right\|_2$. Moreover, the matrix $\mathbf{Q}$ is determined by the synthetic source dipole moments as $\mathbf{Q} = (\tilde{\mathbf{q}}_{\tilde{\mathbf{w}}_1}, \tilde{\mathbf{q}}_{\tilde{\mathbf{w}}_2}, \ldots, \tilde{\mathbf{q}}_{\tilde{\mathbf{w}}_M})$. The minimizer of $\sum_{\ell=1}^{M} c_\ell^2 \omega_\ell^2$ is obtained by implementing the method of Langrangian multipliers, resulting in a uniquely solvable linear system. The number of source dipoles M depends on the source configuration, which is explained in more detail below.

We also test adaptability, i.e., how the number n of the elements in the patch affects the source modeling accuracy for $n = 1, 2, \ldots, 5$. In the simplest case $n = 1$, the sources correspond to the edges of a single tetrahedron (six EW dipoles). For $n = 2, \ldots, 5$, this configuration is extended by including the EW and FI dipoles from the neighboring elements, leading to a total of 10–22 synthetic dipoles (Fig. 2).

In the PBO interpolation scheme, a given dipole position and moment can be estimated with different combinations of the synthetic dipoles (Pursiainen et al., 2016). As a fundamental source configuration we use a set of 22 synthetic FI and EW dipoles corresponding to a five-element patch: a center tetrahedron together with its facial neighbors (Fig. 1). To avoid forward modeling errors due to discontinuities in the electrical conductivity distribution, those elements which do not belong to the gray matter are excluded from the configuration (Fig. 1). That is, in the vicinity of the boundary of the brain, fewer elements and sources are used in the interpolation.

In the partial integration method, the element patch consists of a single element which is assumed to contain the dipole source. The St. Venant approach is to place monopolar sources at the nodes of the element patch, so that their net effect corresponds to that of the given dipole. The ball-like patch is formed as the set of all the elements sharing the node that is closest to the dipole location. This strategy usually results in around 20 elements in an unstructured tetrahedral mesh. Fig. 3 shows that approximately one half of the elements are taken out of the final patch on the gray matter boundary.

2.3. Implementation in duneuro

As a platform of forward computations, we utilized the C++ based toolbox DUNE (Blatt and Bastian, 2007; Blatt et al., 2016; Bastian et al., 2008a; b). In fact, the implementation was created for the *duneuro* module (Nüßing et al., 2016; Engwer et al., 2017; Vorwerk et al., 2017), which is a DUNE based toolbox for bioelectromagnetic (EEG, MEG, tES) forward modeling. The divergence conforming H(div) source model was newly implemented whereas the scripts for the partial integration and St. Venant methods already existed in the toolbox.

As modular platforms, *DUNE/duneuro* are well-suited for implementing the H(div) source model together with the PBO interpolation approach. *DUNE* includes numerous lower level routines for handling the FE mesh and basis functions which can be effortlessly applied in the actual script. In the present case, the most central requirement for the programming environment is the ability to easily find the elements belonging to different tissue compartments and to identify the facial neighbors of a given center tetrahedron. In *DUNE*, these operations can be handled through the basic modules.

The algorithm for the EEG forward modeling numerical analysis with *duneuro* is presented in Fig. 4. The algorithm starts by creating a driver object which serves as the main interface to the *duneuro* module. This is done by defining the grid type, and the nodes, elements, and layer labels and conductivity values for each element. Next, the electrodes are passed to the driver object, and the algorithm can compute the transfer matrix. Then, the dipole set is delivered to the driver, and the source model is selected. After that, the toolbox can compute the potential values at the electrode locations. Furthermore, the analytical solution is calculated, and the statistics are then created for error measures. Finally, the error statistics are illustrated with MATLAB - boxplot[3] function.

[3] MATLAB, version 9.1 (R2016b), The MathWorks Inc., Natick, Massachusetts.

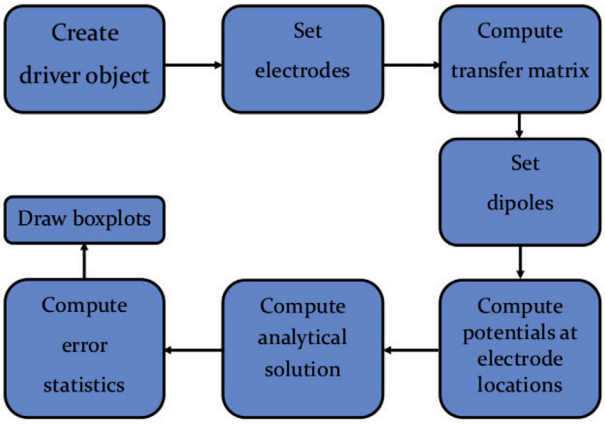

Fig. 4. The general algorithm for *duneuro* EEG forward problem implementation.

The FE mesh was chosen to be an unstructured and conforming tetrahedral mesh based on the *DUNE-ALUGrid* module (Alkämper et al., 2016). The weak form of the forward problem was discretized with the *DUNE-PDELab* module (Bastian et al., 2010).

The linear system was solved using an iterative preconditioned conjugate gradient method (PCG) equipped with an algebraic multigrid preconditioner (AMG) which uses a symmetric successive over relaxation (SSOR) as a smoother (Blatt, 2010). The stopping criteria for the PCG, i.e., the relative residual 2-norm, was set to 10^{-8}.

A source model function was implemented for H(div) sources that form the load vector $\mathbf{f}$ (right-hand side) of the forward problem. It proceeds as follows:

1. The position and moment of a given dipole are send to the source model.
2. *DUNE* detects the element in which the dipole is located and computes the EW source dipoles for that element.
3. The method loops through the neighboring elements with the help of the *intersections* function in *DUNE*, and computes the corresponding FI and EW source dipoles. This is done recursively until the required number of source elements is reached.
4. The generated source dipoles are delivered to the PBO interpolation method, and the resulting coefficients are used for computing the load vector $\mathbf{f}$, which represents the current field approximation in the global mesh.
5. Finally, the load vector $\mathbf{f}$ is passed to a solver that computes the corresponding potential distribution.

2.4. Numerical experiments

The spherical FE mesh applied in this study is presented in Fig. 5. It consists of 5.6 M elements and 0.9 M nodes and altogether six compartments: Brain layers 1–3 (white, dark gray, green), CSF (purple), Skull (blue), and Scalp (yellow). This mesh was designed based on the isotropic four-layered Stok model (Stok, 1987) (Brain, CSF, Skull, Scalp) specifically for evaluating how the source models perform in the 2 mm thick Brain 3 (gray matter) layer (green). The radii and conductivity values for all compartments can be found in Table 1. A similar 1:80 conductivity ratio between the skull and the brain has been recently used, e.g., in (Aydin et al., 2014).

The FE mesh was generated using the Gmsh software,[4] and it was refined towards the surface of the brain. The longest and shortest edge length in the mesh were 3.9 and 0.31 mm, respectively.

The accuracy of the FE solution was measured against the analytical solution, which can be obtained for a multi-layered sphere. Both the analytical and numerical solution were evaluated at 120 electrodes evenly distributed over the scalp layer. We generated two sample sets, each one consisting of 200 dipole sources with random orientations. The dipoles of the first set were located at 1.5 mm distance from the outer gray matter boundary, i.e., at the relative radius (eccentricity) of 98% with respect to the surface of the brain. The second set contained dipoles at 0.078 mm distance, that is, at an eccentricity of 99.9%. Due to the previous study about deeper lying sources by (Pursiainen et al., 2016), the interest was mostly on superficial areas of cortex in this study. That is the reason for considering 1.5 mm and 0.078 mm source dipoles in line with numerical approaches, i.e., RDM and MAG, which demonstrated that the less eccentric sources are, the lower is the numerical error, which leads to more focal sources regarding to the multi-layered sphere model.

2.5. Error measures

The analytical potential values were computed harnessing the method of De Munck and Peters (de Munck and Peters, 1993). The accuracy of the H(div) model was compared to that of the reference techniques, the St. Venant (Buchner et al., 1997; Toupin, 1965) and the partial integration method (Yan et al., 1991; Weinstein et al., 2000). The relative difference (RDM) and magnitude (MAG) measure (Pursiainen et al., 2016), defined below, were evaluated in percents.

$$\mathrm{RDM}(\mathbf{y}_{\mathrm{ana}}, \mathbf{y}_{\mathrm{num}}) = 50 \left\| \frac{\mathbf{y}_{\mathrm{ana}}}{\|\mathbf{y}_{\mathrm{ana}}\|_2} - \frac{\mathbf{y}_{\mathrm{num}}}{\|\mathbf{y}_{\mathrm{num}}\|_2} \right\|_2 \tag{7}$$

$$\mathrm{MAG}(\mathbf{y}_{\mathrm{ana}}, \mathbf{y}_{\mathrm{num}}) = 100 \left(\frac{\|\mathbf{y}_{\mathrm{num}}\|_2}{\|\mathbf{y}_{\mathrm{ana}}\|_2} - 1 \right). \tag{8}$$

The RDM reflects the topographical forward modeling error in terms of location and orientation. The MAG reveals the variations in potential amplitude or, in other words, alterations in the source strength.

The error measures are presented as box plots (Kirkman, 1996) which describe the lower (25%), middle (50%), and upper (75%) quartiles with a box graph. The thicker part shows the inter quartile range (IQR or spread) between 25% and 75% quartile. The median, i.e., the 50% quartile, is shown as a horizontal line in the IQR. The vertical lines, whiskers, show the maximum and minimum values of the dataset. Here the whiskers are limited with the 1.5IQR rule, i.e., their maximal extent is 1.5 times the length of the IQR, and the rest of the dataset is marked as outliers. Furthermore, the statistically significant mutual differences for RDM and MAG values were evaluated with the Mann Whitney U test (Mann and Whitney, 1947) with the confidence level of 95%.

2.6. Inversion test with a realistic geometry

In order to highlight the differences of the examined source models and the impact of the presented numerical forward errors, we performed an inverse investigation in a realistic head model. The motivation was that the adaptive H(div) FEM source model might help to interpret reconstructions by preventing deteriorated (e.g. spotty) inverse results which might occur as a result of minimum norm estimation (MNE) within a thin cortex. A head segmentation of a healthy 24 year old male subject obtained via T1-and T2-weighted magnetic resonance images (Pursiainen et al., 2012) was utilized to test the potential of the present H(div) approach in reconstructing the brain activity. The following seven different isotropic conductivity (S/m) compartments were distinguished: skin (0.43 S/m), the compact and spongious bone of the skull (0.0064 and 0.028 S/m, respectively), cerebrospinal fluid (1.79 S/m), gray matter (0.33 S/m), white matter (0.14 S/m), and eyes (0.505 S/m). Justification of conductivity values can be found, e.g., in (Dannhauer et al., 2011). The

[4] http://gmsh.info.

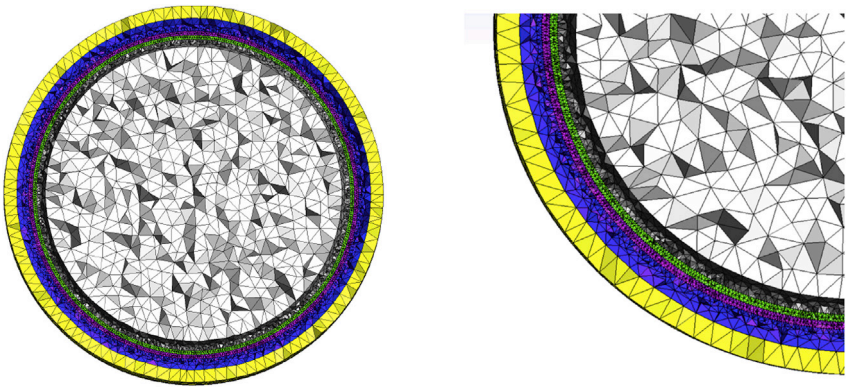

Fig. 5. A visualization of the spherical grid used for modeling.

Table 1
The sphere radii and conductivity values for all mesh compartments.

Compartment	Radius (mm)	Conductivity (S/m)
Scalp	92	0.33
Skull	86	0.0042
CSF	80	1.79
Brain 3 (Gray Matter)	78	0.33
Brain 2	76	0.33
Brain 1	72	0.33

segmentation was discretized by generating a regular tetrahedral grid with the element size 0.85 mm via the open source *Zeffiro* toolbox,[56] Matlab (The MathWorks, Inc.). The total number of elements and nodes in the resulting FE mesh was 37.9 M and 6.45 M, respectively.

The lead field matrix was computed for 0.5 M randomly chosen source positions with Cartesian orientations. Two different source sets (A) and (B) were used. In the first one of these, the sources were placed deep in the gray matter compartment. In the second one, the source positions extended also to the surface of the gray matter, i.e., part of the sources were associated with the surface tetrahedra. The following two current preserving source modeling strategies were tested: (i) non-adaptive H(div), i.e., the basic five-element configuration $n = 5$, and (ii) adaptive H(div) in which the configuration was adapted ($n = 1, 2, \ldots,$ 5) according to the local mesh geometry. Of (i) and (ii), the latter allows a more focal source placement, meaning that the source distribution extends closer to the surface of the gray matter compartment. For comparison, reconstructions for the sets (A) and (B) were also computed with the partial integration and St. Venant source modeling approach. The latter one of these was adapted as shown in Fig. 3 to enable source modeling in the vicinity of the boundary for the set (B).

The measurement data, i.e., the potential values $\mathbf{y}$, were simulated for a normally oriented source in Brodmann area 1 of the right somatosensory cortex (Fig. 6). Gaussian zero mean noise with 5% relative standard deviation with respect to the maximal data entry was added to the simulated measurements. The reconstruction was computed via one and two steps of the iterative alternating sequential (IAS) iteration (Calvetti et al., 2009; Lucka et al., 2012; Pursiainen, 2012) by setting the shape and scaling parameter to 1.5 and 1E-3, respectively. With the present choice of the shape parameter, the one- and two-step IAS estimate constitute an ℓ^2- and ℓ^1-regularized estimate, i.e., a minimum norm and minimum current estimate (MNE and MCE), respectively (Calvetti et al., 2009; Uutela et al., 1999).

[5] https://github.com/sampsapursiainen/zeffiro-interface/wiki.
[6] https://se.mathworks.com/matlabcentral/fileexchange/68285.

3. Results

The results of the numerical analysis have been included in Figs. 7, 8 and 9 as well as Tables 2 and 3.

It can be observed that, for the H(div) model, the forward simulation accuracy increases along with the number of elements in the source configuration. The smallest median RDM (0.28 and 0.26% for 98 and 99.9% eccentricity, respectively) is obtained with the five-element patch. Furthermore, the spread (IQR) of the RDM decreases as the source count grows. The results of the Mann-Whitney test suggest that, compared to the single-element source configuration, a (statistically) significant improvement in RDM can be obtained, when $n \geq 2$ and $n \geq 3$ for the eccentricity of 98 and 99.9%, respectively. For MAG, the spread decreases, when the number of the elements increases, but there is no such clear tendency for the median. The median differences were, however, found to be mainly insignificant based on the Mann-Whitney test.

In comparison between the H(div) approach and the St. Venant and partial integration method, the single-element H(div) was found to yield generally very similar results with the partial integration. At 98% eccentricity, the St. Venant method achieved a median RDM of 0.30% which is close to the value obtained with the five-element divergence conforming scheme. At 99.9% eccentricity, the difference was more obvious in favor of the H(div) model, as the median RDM for the St. Venant approach in that case was 0.44%. With respect to the MAG, the St. Venant was the superior method at 98% eccentricity, but not at 99.9%, where its performance was marginally weaker than that of the five-element H(div). According to the U test, the MAG differences at 99.9% eccentricity were statistically insignificant, and, therefore, those have been omitted in Table 2.

An obvious reason for the deteriorated performance of the St. Venant approach at the eccentricity of 99.9% can be found in Table 3, showing that the source element patch was significantly restricted in that case: the median for the number of elements in the patch was 20 and 10 for 98 and 99.9% eccentricity, respectively. For comparison, maximally one element was restricted out of the patch in the H(div) approach.

In the inversion test involving H(div) sources (Figs. 8 and 9), both the (i) non-adaptive ($n = 5$) and (ii) adaptive ($n = 1, 2, \ldots, 5$) technique enabled reconstructing the synthetic somatosensory source. The smoother reconstruction and superior focality was obtained with the source set (A) which is especially clear in the case of the ℓ^2-estimate. Namely, for (B), the set in which the ℓ^2-estimate essentially differs from zero extends up to 10 mm further away from the actual source position. Nevertheless, the ℓ^1-estimate converges towards the actual source position for both (A) and (B) resulting in a well-localized reconstruction. The results suggest that, of the tested source modeling techniques, the H(div) approach produces, generally, the smoothest distribution, which is more regular in the active area, than what is obtained with the partial integration and St. Venant method. In particular, the H(div)-based

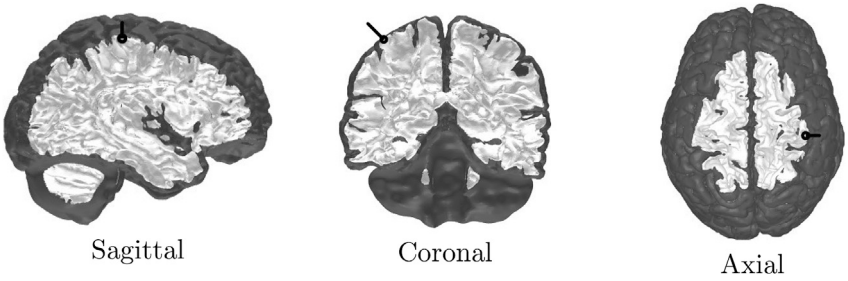

Fig. 6. Placement of a normally oriented source in Brodmann area 1 of the right somatosensory cortex in sagittal, coronal and axial projection (left, center and right, respectively). The actual source position and orientation is shown by the black circle and line segment, respectively.

Table 2
The results of the Mann-Whitney *U* test for restricted source models with *n* elements, for partial integration, and for St. Venant with 200 dipoles. The MAG results have been omitted for 99.9% eccentricity, since all the differences were insignificant in that case.

RDM at 98% eccentricity							
	n = 1	n = 2	n = 3	n = 4	n = 5	PI	St.V.
n = 1		*	*	*	*		*
n = 2	*		*	*	*	*	*
n = 3	*	*		*	*	*	*
n = 4	*	*	*		*	*	
n = 5	*	*	*	*		*	
PI		*	*	*	*		*
St.V.	*	*	*			*	
MAG at 98% eccentricity							
	n = 1	n = 2	n = 3	n = 4	n = 5	PI	St.V.
n = 1		*					*
n = 2	*				*	*	
n = 3							
n = 4							
n = 5		*					*
PI		*					*
St.V.	*				*	*	
RDM at 99.9% eccentricity							
	n = 1	n = 2	n = 3	n = 4	n = 5	PI	St.V.
n = 1			*	*	*		*
n = 2				*	*		*
n = 3	*					*	*
n = 4	*	*				*	*
n = 5	*	*				*	*
PI			*	*	*		*
St.V.	*	*	*	*	*	*	

Table 3
The number of the source elements (source element patch size) for each source model type in the numerical experiments.

At 98% eccentricity				
	min	max	median	mean
PI	1	1	1	1
St. V.	14	36	20	21.31
n = 1	1	1	1	1
n = 2	2	2	2	2
n = 3	3	3	3	3
n = 4	4	4	4	4
n = 5	5	5	5	5
At 99.9% eccentricity				
	min	max	median	mean
PI	1	1	1	1
St. V.	5	17	10	10.57
n = 1	1	1	1	1
n = 2	2	2	2	2
n = 3	3	3	3	3
n = 4	4	4	4	4
n = 5	4	5	4	4.12

reconstruction was the most intense and least spotty near the actual source position in the case (B), i.e., when the source distribution extended to the boundary. Overall, the results suggest that the H(div) approach is more regular and topographically stable compared to St. Venant and partial integration.

4. Discussion

This article presented, validated and evaluated an adaptable open source implementation of the current preserving (divergence conforming) H(div) model (Tanzer et al., 2005; Pursiainen et al., 2016; Bauer et al., 2015) for EEG forward computations (Brette and Destexhe, 2012) in unstructured tetrahedral grids. The H(div) approach is advantageous in modeling the primary current field generated by the neural activity, since it achieves the best balance between realism, focality, numerical accuracy and computational speed with regard to source placement in the thin and geometrically complex gray matter compartment, which is on average only slightly more than 2 mm thick (Griffis et al., 2016; Fischl and Dale, 2000; McGinnis et al., 2011). Especially, this is the case for exceptionally thin cortical compartments as can be found in children, infant and neonate brain research (Li et al., 2014; Hämäläinen et al., 2015; Roche-Labarbe et al., 2008) and/or in pathological situations (Seitz et al., 2014).

A function for the present source model was written for the C++ based *duneuro* library, which is integrated in *DUNE*. This function was evaluated numerically against the competing source models St. Venant (Buchner et al., 1997; Toupin, 1965; Medani et al., 2015; Medani, 2016) and partial integration (Yan et al., 1991; Weinstein et al., 2000), which are also implemented in *duneuro*. *duneuro* and *DUNE* were found to be suitable platforms for our research purpose, as they are openly accessible state-of-the-art modeling packages for bioelectromagnetic (EEG, MEG, tES) forward modeling (Nüßing, 2018; Nüßing et al., 2016; Engwer et al., 2017; Vorwerk et al., 2017), and, more generally, for solving partial differential equations (Blatt and Bastian, 2007; Blatt et al., 2016; Bastian et al., 2008a; b), respectively. Their modular structures allow easy operation of the lower level code and, thereby, enable the handling of the FE mesh and basic functions effortlessly such as, e.g., tracking the local mesh structure in the neighborhood of a given element, which was essential for this implementation. *duneuro* also offers mathematically advanced FE based EEG, MEG and tES forward modeling: In addition to the present classical continuous Galerkin (CG-FEM) approach, it also offers discontinuous Galerkin (DG-FEM) (Engwer et al., 2017), unfitted FEM approaches such as CUTFEM (Nüßing, 2018) and unfitted DG-FEM (Nüßing et al., 2016), and Mixed-FEM computations (Vorwerk et al., 2017). Especially, in the latter one of these, the primary source current is inherently assumed to be divergence conforming. Hence, a further optimization of the H(div) model can be considered.

Our code was evaluated numerically using a six-compartment spherical domain obtained by subdividing the brain compartment of the classical isotropic four-layered Stok model (Stok, 1987) into three

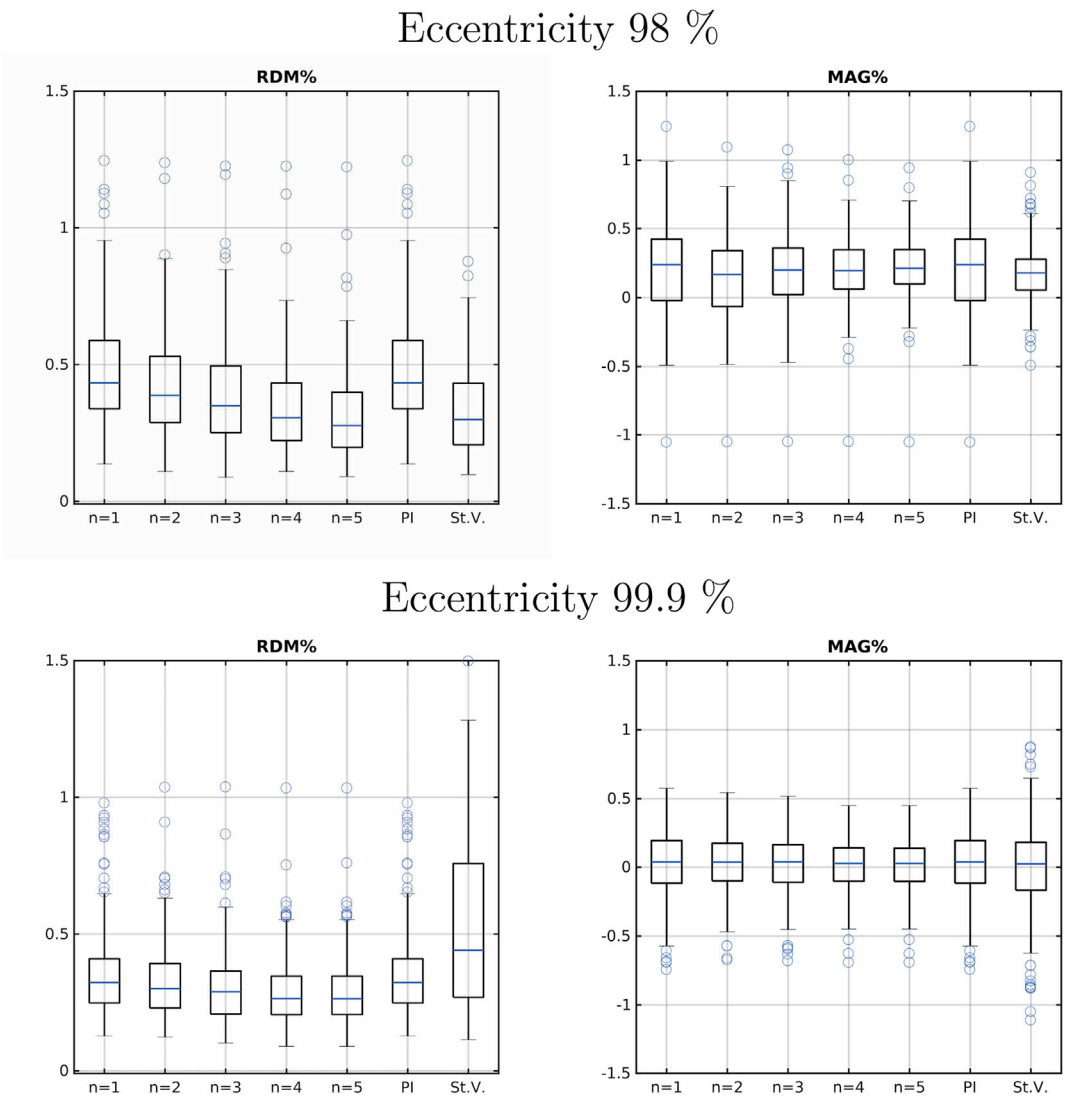

Fig. 7. The RDM and MAG errors for divergence conforming source models with n elements, for partial integration and for St. Venant tested with 200 dipoles at eccentricity 98% (top row) and 99.9% (bottom row).

parts. The outermost brain compartment modeled an only 2 mm thin gray matter layer. Akin to a realistic setting, all the elements in the patch of the source configuration belonged to this compartment. If necessary, a restricted patch was used. Our goal was to find out how the H(div) forward model performs in the vicinity of the gray matter boundary, where a restriction has to be made and the discontinuity of the electrical conductivity distribution between the brain and the CSF compartment can diminish the accuracy of the forward simulation. The relative difference and magnitude measures (RDM and MAG) were evaluated for two sets of 200 dipoles with random positions and orientations. One of these sets was located at the eccentricity of 98%, i.e., a source depth of 1.5 mm, which is typical in a realistic scenario. The other one concerned the eccentricity of 99.9%, i.e., an extraordinary shallow depth of about 0.1 mm, reflecting an exceptional situation in which the element patch of the source current needs to be placed very close to the surface of the gray matter. In realistic volume conductor modeling, these capabilities are vital as the cortex of healthy subjects is on average only slightly more than 2 mm thick (Griffis et al., 2016; Fischl and Dale, 2000; McGinnis et al., 2011) or even thinner such as in children, infant or neonate studies (Li et al., 2014; Hämäläinen et al., 2015; Roche-Labarbe et al., 2008), in pathological situations (Seitz et al., 2014) or in just segmentation related issues.

Of the present evaluated source models, the H(div) approach was found to be overall superior compared to the St. Venant and partial integration. With respect to RDM, the performance differences between the methods were significant based on the results of both boxplot analysis and the Mann-Whitney's significance test (U test). Nevertheless, the MAG differences were found to be mainly not crucial, suggesting that all three models yield essentially the same performance with respect to the magnitude.

Concentrating on the RDM, the modeling accuracy was observed to increase along with the number of elements in the source patch. The results obtained with a single-element ($n = 1$) patch were largely similar to those produced by the partial integration routine which is also based on a single element. It seems that a statistically significant improvement compared to the simplest $n = 1$ case can be obtained using a patch of three or more elements regardless of the eccentricity. The most significant difference to the St. Venant method was observed at 99.9% eccentricity which necessitated restricting the St. Venant's element patch into one half of its normal composition (a ball-like object cut into half) and, consequently, led to a considerably deteriorated RDM. Nevertheless, for H(div), only a minor single-element restriction was needed without a notable decrease in the performance. Thus, it seems that the patch formed around a given center element is advantageous with regard to source placement close to a boundary.

Skull conductivity is an important parameter in EEG source analysis.

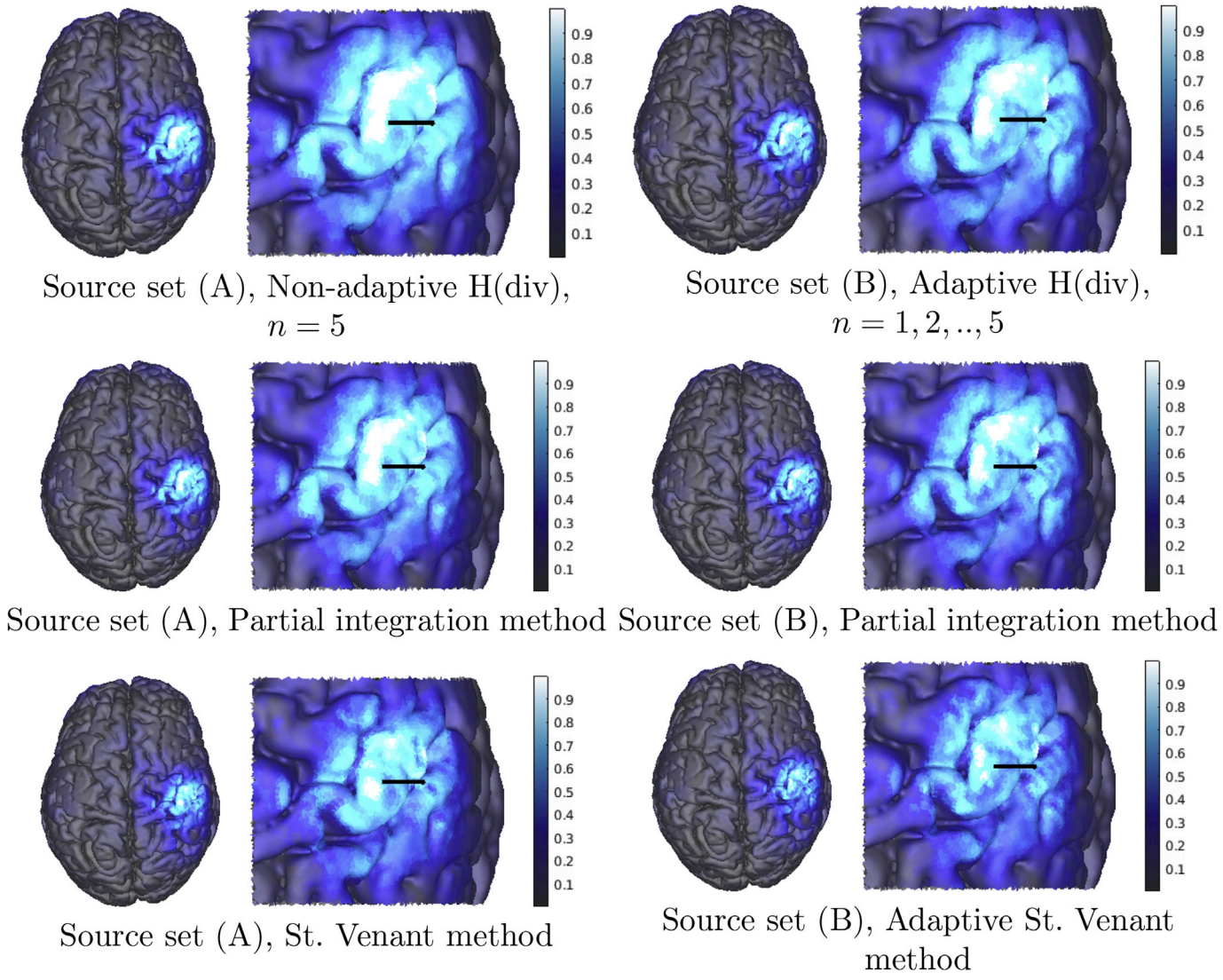

Fig. 8. The ℓ^2-regularized reconstructions (minimum norm estimates) of the primary current distribution for two source sets (A) and (B) in which the sources are positioned deep and everywhere in the gray matter compartment, respectively. The top row shows the results obtained with (i) the H(div) ($n = 5$) and (ii) the adaptive ($n = 1, 2, .., 5$) H(div) source model (left and right, respectively). The center row corresponds to the partial integration method, and the bottom row to the non-adaptive and adaptive version of the St. Venant method, respectively. Notice that as the partial integration method utilizes only a single element, it cannot be adapted akin to the H(div) and St. Venant model. The actual source position and orientation is shown by the left tip and the stem of the black line segment, respectively.

In the present multi-layered simulation study a conductivity of 0.0042 S/m for the skull layer and 0.33 S/m for the gray matter layer was chosen, i.e., a skull/brain conductivity ratio of about 1:80 was considered. This is the classical ratio (Homma et al., 1995), which is still used as a default in commercial software packages, see, e.g, (Fuchs et al., 1998). For higher skull/brain conductivity ratios as proposed by (Dannhauer et al., 2011), all presented numerical errors and, therefore, also the differences between the examined dipole modeling approaches decrease in both normal and tangential orientations. A better way for skull modeling might, however, be to distinguish the lower conducting skull compacta and higher conducting skull spongiosa compartments (Dannhauer et al., 2011; Montes-Restrepo et al., 2014) and to individually estimate their conductivity parameters. This has recently been done using a skull conductivity calibration procedure based on combined somatosensory evoked potential (SEP) and field (SEF) measurements, where estimated conductivity values were 0.0024 S/m and 0.0084 S/m in one (Aydin et al., 2014) and 0.0033 S/m and 0.0116 S/m in another epilepsy patient (Aydin et al., 2017) for the skull compacta and spongiosa compartments, respectively. This shows that individual differences in skull conductivity parameters have to be expected, which will significantly influence EEG based source analysis. In addition to the skull, also the white matter is important regarding the source modeling accuracy, especially, since the real white matter conductivity includes anisotropy (Wolters et al., 2006; Güllmar et al., 2010; Vorwerk et al., 2014). The actual effect of the anisotropy to the accuracy may be expected to depend strongly on source position and orientation, whereas the current model only reflects the average effect. Overall, we expect that the mutual performances between the investigated source models will be maintained for a wide range of conductivities, since the conductivity distribution is primarily a parameter for the system matrix, whereas the source model mainly reflects the accuracy of the right-hand-side vector of the forward problem.

Our validation results together with the inversion test suggest that our implementation can be beneficial for complex 3D meshes. It allows an extremely focal single-element source placement with the accuracy of the partial integration, which can be necessary at some locations in a realistic volume conductor. Additionally, if the local geometry allows using the full source configuration, then the accuracy of the St. Venant can be surpassed. Thus, a close to optimal accuracy can be achieved in each

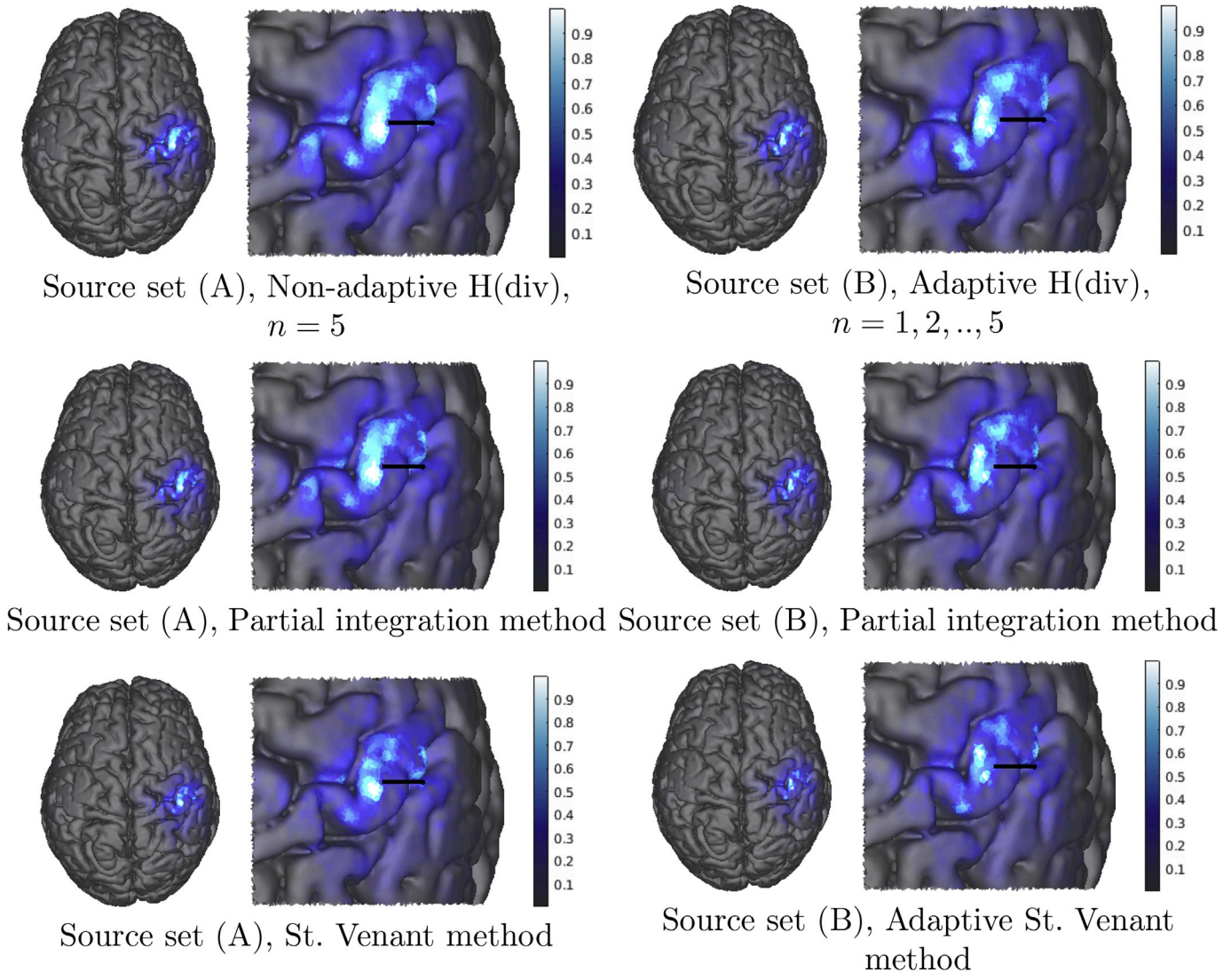

Fig. 9. The ℓ^1-regularized reconstructions (minimum current estimates) of the primary current distribution for two source sets (A) and (B).

situation without the need to choose between different source models. Based on the present numerical analysis, the non-adaptive H(div) source modeling approach (i) is more robust than the adaptive one (ii) and is, therefore, preferable for a normal cortex thickness, which is on average 2.3 mm (Griffis et al., 2016; McGinnis et al., 2011; Fischl and Dale, 2000). However, (ii) was found to be sufficient for special cases e.g. with extremely thin cortices.

In de Munck et al. (1988), it was presented that the mathematical point dipole, due to its over-focal nature, results in modest, but systematic errors for depth localization when compared to a more realistic and slightly more extended source model. Using the subtraction approach, the point dipole can also be modeled with its full focality in a FEM framework, but it is known that numerical errors might get significant in thin cortices where sources are very close to the next conductivity discontinuity and that it is currently still computationally expensive (Bertrand et al., 1991; Awada et al., 1997; Marin et al., 1998; Schimpf et al., 2002; Drechsler et al., 2009). In this paper, we showed that H(div)-type source models can be constructed in a way that is more realistic than the mathematical point dipole with regard to extent, but as accurate in multi-layer sphere model validations. In addition, the H(div) source models were found to be also focal enough to be induced in even thin cortices. As already mentioned, this feature is crucial in healthy subjects, but especially in children, infant and neonate EEG brain research or in pathological situations. In summary, the best H(div) source thus has the best balance between numerical accuracy, computational efficiency and modeling accuracy, i.e., focal enough to be usable in thin cortices, but less focal and thus more realistic than the mathematical point dipole.

An important future work will be to evaluate the present current preserving source model implementation in a group study with real EEG data and realistic FEM head models. To do so, the *duneuro* library will be coupled, for instance, with the *FieldTrip*[7] or *BrainStorm*[8] toolboxes, similar to the interface that has already been realized for the *duneuro*-predecessor *SimBio*[9] (Vorwerk et al., 2018). Likewise, both Python and Matlab bindings already exist for *duneuro*. Further analysis of the relationship between the presented source model and realistic physiological structures, e.g., thin cortices and anisotropy, will be necessary.

5. Conclusions

The purpose of this study was to improve EEG source analysis using finite element method (FEM) head volume conductor models that extend

[7] FieldTrip: http://www.fieldtriptoolbox.org.
[8] BrainStorm: http://neuroimage.usc.edu/brainstorm.
[9] SimBio: https://www.mrt.uni-jena.de/simbio.

the standard three compartment approach, and are able to take brain tissue inhomogeneity (gray and white matter and cerebrospinal fluid) into account. The focus was on determining the performance of the present current preserving H(div) source model which was implemented into the open source *duneuro* library for FEM forward modeling in bioelectromagnetism, and validated through numerical experiments for source configurations corresponding to $n = 1, \ldots, n = 5$ elements in the FEM mesh. The accuracy of the model was measured against an analytical solution in a multi-layer sphere model. The performance achieved was evaluated with two competing methods, partial integration and St. Venant. The results obtained within a spherical multi-layered domain suggest that our new approach provides a solid way to model the primary current distribution in the thin cortical compartment, and even in situations of exceptionally thin cortices. A superior performance was achieved in the vicinity of the outer gray matter boundary, in particular, as compared to the St. Venant reference method. The modeling precision was found to improve significantly as the size of the source modeling patch grew from one to three or more elements. No significant performance differences were observed between the four- and five-element patches when the sources were located close to the outer gray matter boundary. We also performed an inversion test suggesting that our development can be used to improve EEG forward modeling for realistic multi-compartment head models, and it might be of special importance in situations of thin cortices, e.g., in children and/or pathological applications.

Acknowledgements

TM was supported by SP's Tenure Track project funding, Tampere University of Technology, Finland. TM, DU, AR, and SP were supported by the Academy of Finland Key project (project 305055) and by the Academy of Finland Centre of Excellence in Inverse Problems Research (312341). AN, CE and CHW were partially supported by EU project ChildBrain (Marie Curie Innovative Training Networks, grant agreement 641652), by the Deutsche Forschungsgemeinschaft, project WO1425/7-1, by the DFG priority program SPP1665, project WO1425/5-2, and the DFG Cluster of Excellence 1003 (DFG EXC 1003 Cells in Motion). AR, CHW, and SP were supported by the Deutscher Akademischer Austauschdienst via funding from the Bundesministerium für Bildung und Forschung.

References

Ainsworth, M., Coyle, J., 2003. Hierarchic finite elements for unstructured tetrahedral meshes. Int. J. Numer. Meth. Eng. 58, 2103–2130.
Alkämper, M., Dedner, A., Klöfkorn, R., Nolte, M., 2016. The DUNE-ALUGrid module. Archive of Numerical Software 4 (1).
Awada, K.A., Jackson, D.R., Williams, J.T., Wilton, D.R., Baumann, S.B., Papanicolaou, A.C., 1997. Computational aspects of finite element modeling in EEG source localization. IEEE (Inst. Electr. Electron. Eng.) Trans. Biomed. Eng. 44 (8), 736–752.
Aydin, Ü., Rampp, S., Wollbrink, A., Kugel, H., Cho, J.-H., Knösche, T., Grova, C., Wellmer, J., Wolters, C., 2017. Zoomed MRI guided by combined EEG/MEG source analysis: a multimodal approach for optimizing presurgical epilepsy work-up and its application in a multi-focal epilepsy patient case study. Brain Topogrry 30 (4), 417–433.
Aydin, Ü., Vorwerk, J., Küpper, P., Heers, M., Kugel, H., Galka, A., Hamid, L., Wellmer, J., Kellinghaus, C., Rampp, S., et al., 2014. Combining EEG and MEG for the reconstruction of epileptic activity using a calibrated realistic volume conductor model. PLoS One 9 (3) e93154.
Bastian, P., Blatt, M., Dedner, A., Engwer, C., Klöfkorn, R., Kornhuber, R., Ohlberger, M., Sander, O., 2008a. A generic grid interface for parallel and adaptive scientific computing. Part I: abstract framework. Computing 82 (2–3), 103–119.
Bastian, P., Blatt, M., Dedner, A., Engwer, C., Klöfkorn, R., Kornhuber, R., Ohlberger, M., Sander, O., 2008b. A generic grid interface for parallel and adaptive scientific computing. Part II: implementation and tests in DUNE. Computing 82 (2–3), 121–138.
Bastian, P., Heimann, F., Marnach, S., 2010. Generic implementation of finite element methods in the distributed and unified numerics environment (DUNE). Kybernetika 46 (2), 294–315. URL. http://eudml.org/doc/197255.
Bauer, M., Pursiainen, S., Vorwerk, J., Köstler, H., Wolters, C.H., 2015. Comparison study for Whitney (Raviart-Thomas) type source models in finite element method based EEG forward modeling. IEEEEngineering(Inst. Electr. Electron. Eng.) Trans. Biomed. Eng. 62 (11), 2648–2656.
Bertrand, O., Thévenet, M., Perrin, F., 1991. 3D finite element method in brain electrical activity studies. In: Nenonen, J., Rajala, H., Katila, T. (Eds.), Biomagnetic Localization and 3D Modelling. Report of the Dep. of Tech.Physics. Helsinki University of Technology, pp. 154–171.
Blatt, M., 2010. A Parallel Algebraic Multigrid Method for Elliptic Problems with Highly Discontinuous Coefficients. Dissertation, Heidelberg University. URL. http://www.ub.uni-heidelberg.de/archiv/10856.
Blatt, M., Bastian, P., 2007. The Iterative Solver Template Library. Springer Berlin Heidelberg, pp. 666–675.
Blatt, M., Burchardt, A., Dedner, A., Engwer, C., Fahlke, J., Flemisch, B., Gersbacher, C., Gräser, C., Gruber, F., Grüninger, C., Kempf, D., Klöfkorn, R., Malkmus, T., Müthing, S., Nolte, M., Piatkowski, M., Sander, O., 2016. The distributed and unified numerics environment, version 2.4. Archive of Numerical Software 4 (100), 13–29.
Braess, D., 2001. Finite Elements. Cambridge University Press, Cambridge.
Brette, R., Destexhe, A., 2012. Handbook of Neural Activity Measurement. Cambridge University Press, New York.
Buchner, H., Knoll, G., Fuchs, M., Rienäcker, A., Beckmann, R., Wagner, M., Silny, J., Pesch, J., 1997. Inverse localization of electric dipole current sources in finite element models of the human head. Electroencephalogr. Clin. Neurophysiol. 102 (4), 267–278.
Calvetti, D., Hakula, H., Pursiainen, S., Somersalo, E., 2009. Conditionally Gaussian hypermodels for cerebral source localization. SIAM J. Imag. Sci. 2 (3), 879–909.
Dannhauer, M., Lanfer, B., Wolters, C.H., Knösche, T.R., 2011. Modeling of the human skull in EEG source analysis. Hum. Brain Mapp. 32, 1383–1399.
de Munck, J., Peters, M., 1993. A fast method to compute the potential in the multisphere model. IEEE Trans. Biomed. Eng. 40 (11), 1166–1174.
de Munck, J., van Dijk, B., Spekreijse, H., 1988. Mathematical dipoles are adequate to describe realistic generators of human brain activity 35 (11), 960–966.
Drechsler, F., Wolters, C., Dierkes, T., Si, H., Grasedyck, L., 2009. A full subtraction approach for finite element method based source analysis using constrained delaunay tetrahedralisation. Neuroimage 46 (4), 1055–1065.
Engwer, C., Vorwerk, J., Ludewig, J., Wolters, C.H., 2017. A discontinuous Galerkin method to solve the EEG forward problem using the subtraction approach. SIAM J. Sci. Comput. 39 (1). URL. http://epubs.siam.org/doi/abs/10.1137/15M1048392.
Fischl, B., Dale, A.M., 2000. Measuring the thickness of the human cerebral cortex from magnetic resonance images. Proc. Natl. Acad. Sci. Unit. States Am. 97 (20), 11050–11055.
Fuchs, M., Wagner, M., Wischmann, H.-A., Köhler, T., Theißen, A., Drenckhahn, R., Buchner, H., 1998. Improving source reconstructions by combining bioelectric and biomagnetic data. Clin. Neurophysiol. 107 (2), 93–111.
Gencer, N., Acar, C., 2004. Sensitivity of EEG and MEG measurements to tissue conductivity. Phys. Med. Biol.
Griffis, J.C., Burge, W.K., Visscher, K.M., 2016. Age-dependent cortical thinning of peripheral visual field representations in primary visual cortex. Front. Aging Neurosci. 8, 248.
Güllmar, D., Haueisen, J., Reichenbach, J., 2010. Influence of anisotropic electrical conductivity in white matter tissue on the EEG/MEG forward and inverse solution. A high-resolution whole head simulation study. NeuroImage 145–163. https://doi.org/10.1016/j.neuroimage.2010.02.014.
Hallez, H., Vanrumste, B., Grech, R., Muscat, J., De Clercq, W., Vergult, A., D'Asseler, Y., Camilleri, K.P., Fabri, S.G., Van Huffel, S., et al., 2007. Review on solving the forward problem in EEG source analysis. J. NeuroEng. Rehabil. 4 (1), 46.
Hämäläinen, J.A., Lohvansuu, K., Ervast, L., Leppänen, P.H., 2015. Event-related potentials to tones show differences between children with multiple risk factors for dyslexia and control children before the onset of formal reading instruction. Int. J. Psychophysiol. 95 (2), 101–112.
Haueisen, J., Tuch, D., Ramon, C., Schimpf, P., Wedeen, V., George, J., Belliveau, J., 2002. The influence of brain tissue anisotropy on human EEG and MEG. Neuroimage 15, 159–166.
Homma, S., Musha, T., Nakajima, Y., Okamoto, Y., Blom, S., Flink, R., Hagbarth, K.-E., 1995. Conductivity ratios of the scalp-skull-brain head model in estimating equivalent dipole sources in human brain. Neurosci. Res. 22 (1), 51–55.
Kirkman, T., 1996. Statistics to Use. URL. http://www.physics.csbsju.edu/stats/. (Accessed 2 August 2017).
Li, G., Nie, J., Wang, L., Shi, F., Gilmore, J.H., Lin, W., Shen, D., 2014. Measuring the dynamic longitudinal cortex development in infants by reconstruction of temporally consistent cortical surfaces. Neuroimage 90, 266–279.
Lucka, F., Pursiainen, S., Burger, M., Wolters, C.H., 2012. Hierarchical bayesian inference for the EEG inverse problem using realistic FE head models: depth localization and source separation for focal primary currents. Neuroimage 61 (4), 1364–1382.
Mann, H.B., Whitney, D.R., 1947. On a test of whether one of two random variables is stochastically larger than the other. Ann. Math. Stat. 18 (1), 50–60. URL. https://doi.org/10.1214/aoms/1177730491.
Marin, G., Guerin, C., Baillet, S., Garnero, L., Meunier, G., 1998. Influence of skull anisotropy for the forward and inverse problem in EEG: simulation studies using the FEM on realistic head models. Hum. Brain Mapp. 6, 250–269.
McGinnis, S.M., Brickhouse, M., Pascual, B., Dickerson, B.C., 2011. Age-related changes in the thickness of cortical zones in humans. Brain Topogr. 24 (3–4), 279.
Medani, T., 2016. Contribution a l'amelioration du modele de source dans la methode des elements finis pour la resolution du probleme direct en electroencephalographie. PhD thesis. Universite Pierre et Marie Curie - Paris, Paris, France. VI. NNT : 2016PA066166.
Medani, T., Lautru, D., Ren, Z., Schwartz, D., Sou, G., Apr, 2015. Modelling of brain sources using the modified saint Venant's method in FEM resolution of EEG forward

problem. In: Conference IEEE EMBS Conference on Neural Engineering 2015. 7th International IEEE EMBS Conference on Neural Engineering. Montpellier, France.
Montes-Restrepo, V., van Mierlo, P., Strobbe, G., Staelens, S., Vandenberghe, S., Hallez, H., 2014. Influence of skull modeling approaches on EEG source localization. Brain Topogr. 27, 95–111.
Nüßing, A., 2018. Fitted and Unitted Finite Element Methods for Solving the EEG Forward Problem. dissertation. Ph.D. thesis, Westfälische Wilhelms-Universität Münster, Germany.
Nüßing, A., Wolters, C., Brinck, H., Engwer, C., 2016. The unfitted discontinuous galerkin method for solving the EEG forward problem. IEEE Trans. Biomed. Eng. 63 (12), 2564–2575.
Papageorgakis, C., 2017. Patient Specific Conductivity Models: Characterization of the Skull Bones. Modeling and Simulation. Universite Cote d'Azur. URL. https://hal.inria.fr/tel-01662075.
Pursiainen, S., 2012. Raviart–thomas-type sources adapted to applied eeg and meg: implementation and results. Inverse Probl. 28 (6), 065013.
Pursiainen, S., Lucka, F., Wolters, C., 2012. Complete electrode model in EEG: relationship and differences to the point electrode model. Phys. Med. Biol. 57 (4), 999.
Pursiainen, S., Vorwerk, J., Wolters, C., 2016. Electroencephalography (EEG) forward modeling via H(div) finite element sources with focal interpolation. Phys. Med. Biol. 61 (24), 8502–8520.
Ramon, C., Schimpf, P., Haueisen, J., 2006. Influence of head models on EEG simulations and inverse source localizations. Biomed. Eng. Online 5 (10).
Roche-Labarbe, N., Aarabi, A., Kongolo, G., Gondry-Jouet, C., Dümpelmann, M., Grebe, R., Wallois, F., 2008. High-resolution electroencephalography and source localization in neonates. Hum. Brain Mapp. 29, 167–176.
Schimpf, P., Ramon, C., Haueisen, J., 2002. Dipole models for the EEG and MEG. IEEE Trans. Biomed. Eng. 49 (5), 409–418.
Seitz, J., Buehren, K., von Polier, G., Heussen, N., Herpertz-Dahlmann, B., Konrad, K., 2014. Morphological Changes in the Brain of Acutely Ill and Weight-recovered Patients with Anorexia Nervosa: a Meta-analysis and Qualitative Review, 42, pp. 7–18, 01.
Stok, C.J., 1987. The influence of model parameters on EEG/MEG single dipole source estimation. IEEE Trans. Biomed. Eng. 34, 289–296.
Tanzer, O., Järvenpää, S., Nenonen, J., Somersalo, E., 2005. Representation of bioelectric current sources using Whitney elements in the finite element method. Phys. Med. Biol. 50, 3023–3039.
Toupin, R., 1965. Saint-Venant's principle. Arch. Ration. Mech. Anal. 18 (2), 83–96.
Uutela, K., Hämäläinen, M., Somersalo, E., 1999. Visualization of magnetoencephalographic data using minimum current estimates. Neuroimage 10, 173–180.
Vorwerk, J., Cho, J.H., Rampp, S., Hamer, H., Knösche, T.R., Wolters, C.H., 2014. A guideline for head volume conductor modeling in EEG and MEG. Neuroimage 100, 590–607.
Vorwerk, J., Clerc, M., Burger, M., Wolters, C., 2012. Comparison of boundary element and finite element approaches to the EEG forward problem. Biomed. Eng./Biomed. Tech. 57 (SI-1 Track-O), 795–798. https://doi.org/10.1515/bmt-2012-4152.
Vorwerk, J., Engwer, C., Pursiainen, S., Wolters, C.H., 2017. A mixed finite element method to solve the EEG forward problem. IEEE Trans. Med. Imag. 36 (4), 930–941.
Vorwerk, J., Oostenveld, R., Piastra, M.C., Magyari, L., Wolters, C.H., 2018. The FieldTrip-Simbio pipeline for EEG forward solutions. Biomed. Eng. Online 17 (37).
Weinstein, D., Zhukov, L., Johnson, C., 2000. Lead-field bases for electroencephalography source imaging. Ann. Biomed. Eng. 28 (9), 1059–1065.
Wolters, C.H., Anwander, A., Tricoche, X., Weinstein, D., Koch, M.A., MacLeod, R.S., 2006. Influence of tissue conductivity anisotropy on EEG/MEG field and return current computation in a realistic head model: a simulation and visualization study using high-resolution finite element modeling. NeuroImage 30 (3), 813–826.
Yan, Y., Nunez, P.L., Hart, R.T., 1991. Finite-element model of the human head: scalp potentials due to dipole sources. Med. Biol. Eng. Comput. 29 (5), 475–481.